First direct observation of spin textures in topological insulators : Spin-resolved ARPES as a probe of topological quantum spin Hall and Berry's phase effects

D. Hsieh,[1] Y. Xia,[1] L. Wray,[1] D. Qian,[1] A. Pal,[1] J. H. Dil,[2,3] F. Meier,[2,3] J. Osterwalder,[3] G. Bihlmayer,[4] C. L. Kane,[5] Y. S. Hor,[6] R. J. Cava,[6] and M. Z. Hasan[1,7]

[1]*Joseph Henry Laboratories of Physics,*
Princeton University, Princeton, NJ 08544, USA

[2]*Swiss Light Source, Paul Scherrer Institute, CH-5232, Villigen, Switzerland*

[3]*Physik-Institut, Universität Zürich-Irchel, 8057 Zürich, Switzerland*

[4]*Institut für Festkörperforschung, Forschungszentrum Jülich, D-52425 Jülich, Germany*

[5]*Department of Physics and Astronomy,*
University of Pennsylvania, Philadelphia, PA 19104, USA

[6]*Department of Chemistry, Princeton University, Princeton, NJ 08544, USA*

[7]*Princeton Center for Complex Materials,*
*Princeton University, Princeton, NJ 08544, USA**

(Dated: First submitted to Science on July 22nd, 2008)

A topologically ordered material is characterized by a rare quantum organization of electrons that evades the conventional spontaneously broken symmetry based classification of condensed matter. Exotic spin transport phenomena such as the dissipationless quantum spin Hall effect have been speculated to originate from a novel topological order whose identification requires a spin sensitive measurement, which does not exist to this date in any system (neither in Hg(Cd)Te quantum wells nor in the topological insulator BiSb). Using spin-ARPES in a Mott polarimetric mode, we probe the spin degrees of freedom of these quantum spin Hall states and demonstrate that topological quantum numbers are uniquely determined from spin texture imaging measurements. Applying this method to the $Bi_{1-x}Sb_x$ series, we identify the origin of its novel order and unusual chiral properties. These results taken together constitute the first observation of surface electrons collectively carrying a geometrical quantum Berry's phase and definite chirality (mirror Chern number, $n_M = -1$), which are the key electronic properties for realizing topological computing bits with intrinsic spin Hall-like topological phenomena. Our spin-resolved results not only provides the first clear proof of a topological insulating state in nature but also demonstrate the utility of spin-resolved-ARPES technique in measuring the quantum spin Hall phases of matter.

*Electronic address: mzhasan@Princeton.edu

Ordered phases of matter such as a superfluid or a ferromagnet are usually associated with the breaking of a symmetry and are characterized by a local order parameter [1], and the typical experimental probes of these systems are sensitive to order parameters. The discovery of the quantum Hall effects in the 1980s revealed a new and rare type of order that is derived from an organized collective quantum motion of electrons [2-4]. These so-called "topologically ordered phases" do not exhibit any symmetry breaking and are characterized by a topological number [5] as opposed to a local order parameter. The classic experimental probe of topological quantum numbers is magneto-transport, where measurements of the quantization of Hall conductivity $\sigma_{xy} = ne^2/h$ (where e is the electric charge and h is Planck's constant) reveals the value of the topological number n that characterizes the quantum Hall effect state [6].

Recent theoretical and experimental studies suggest that a new class of quantum Hall-like topological phases can exist in spin-orbit materials without external magnetic fields, with interest centering on two examples, the "quantum spin Hall insulator" [7-9] and the "strong topological insulator" [10,11]. Their topological order is believed to give rise to unconventional spin physics at the sample edges or surfaces with potential applications ranging from dissipationless spin currents [12] to topological (fault-tolerant) quantum computing [13]. However, unlike conventional quantum Hall systems, these novel topological phases do not necessarily exhibit a quantized charge or spin response ($\sigma_{xy} \neq ne^2/h$) [14,15]. In fact, the spin polarization is not a conserved quantity in a spin-orbit material. Thus, their topological quantum numbers, the analogues of n, cannot be measured via the classic von Klitzing-type [2] transport methods.

Here we show that spin-resolved angle-resolved photoemission spectroscopy (spin-ARPES) can perform analogous measurements for topological metals and insulators. We measured all of the topological numbers for $Bi_{1-x}Sb_x$ and provide an identification of its spin-texture, which heretofore was unmeasured despite its surface states having been observed [10]. The measured spin texture reveals the existence of a non-zero geometrical quantum phase (Berry's phase [16,17]) and the handedness or chiral properties. More importantly, this technique enables us to investigate aspects of the metallic regime of the $Bi_{1-x}Sb_x$ series, such as spin properties in pure Sb, which are necessary to determine the microscopic origin of topological order. Our measurements on pure metallic Sb show that its surface carries a geometrical (Berry's) phase and chirality property unlike the conventional spin-orbit metals

3

such as gold (Au), which has zero net Berry's phase and no net chirality [18].

Strong topological materials are distinguished from ordinary materials such as gold by a topological quantum number, $\nu_0 = 1$ or 0 respectively [14,15]. For $Bi_{1-x}Sb_x$, theory has shown that ν_0 is determined solely by the character of the bulk electronic wave functions at the L point in the three-dimensional (3D) Brillouin zone (BZ). When the lowest energy conduction band state is composed of an antisymmetric combination of atomic p-type orbitals (L_a) and the highest energy valence band state is composed of a symmetric combination (L_s), then $\nu_0 = 1$, and vice versa for $\nu_0 = 0$ [11]. Although the bonding nature (parity) of the states at L is not revealed in a measurement of the bulk band structure, the value of ν_0 can be determined from the spin-textures of the surface bands that form when the bulk is terminated. In particular, a $\nu_0 = 1$ topology requires the terminated surface to have a Fermi surface (FS) [1] that supports a non-zero Berry's phase (odd as opposed to even multiple of π), which is not realizable in an ordinary spin-orbit material.

In a general inversion symmetric spin-orbit insulator, the bulk states are spin degenerate because of a combination of space inversion symmetry $[E(\vec{k},\uparrow) = E(-\vec{k},\uparrow)]$ and time reversal symmetry $[E(\vec{k},\uparrow) = E(-\vec{k},\downarrow)]$. Because space inversion symmetry is broken at the terminated surface, the spin degeneracy of surface bands can be lifted by the spin-orbit interaction [19-21]. However, according to Kramers theorem [16], they must remain spin degenerate at four special time reversal invariant momenta $(\vec{k}_T = \bar{\Gamma}, \bar{M})$ in the surface BZ [11], which for the (111) surface of $Bi_{1-x}Sb_x$ are located at $\bar{\Gamma}$ and three equivalent $\bar{M}$ points [see Fig.1(A)].

Depending on whether ν_0 equals 0 or 1, the Fermi surface pockets formed by the surface bands will enclose the four $\vec{k}_T$ an even or odd number of times respectively. If a Fermi surface pocket does not enclose $\vec{k}_T$ $(= \bar{\Gamma}, \bar{M})$, it is irrelevant for the topology [11,20]. Because the wave function of a single electron spin acquires a geometric phase factor of π [16] as it evolves by 360° in momentum space along a Fermi contour enclosing a $\vec{k}_T$, an odd number of Fermi pockets enclosing $\vec{k}_T$ in total implies a π geometrical (Berry's) phase [11]. In order to realize a π Berry's phase the surface bands must be spin-polarized and exhibit a partner switching [11] dispersion behavior between a pair of $\vec{k}_T$. This means that any pair of spin-polarized surface bands that are degenerate at $\bar{\Gamma}$ must not re-connect at $\bar{M}$, or must separately connect to the bulk valence and conduction band in between $\bar{\Gamma}$ and $\bar{M}$. The partner switching behavior is realized in Fig. 1(C) because the spin down band connects to

and is degenerate with different spin up bands at $\bar{\Gamma}$ and $\bar{M}$. The partner switching behavior is realized in Fig. 2(A) because the spin up and spin down bands emerging from $\bar{\Gamma}$ separately merge into the bulk valence and conduction bands respectively between $\bar{\Gamma}$ and $\bar{M}$.

We first investigate the spin properties of the topological insulator phase. Spin-integrated ARPES [19] intensity maps of the (111) surface states of insulating $Bi_{1-x}Sb_x$ taken at the Fermi level (E_F) [Figs 1(D)&(E)] show that a hexagonal FS encloses $\bar{\Gamma}$, while dumbbell shaped FS pockets that are much weaker in intensity enclose $\bar{M}$. By examining the surface band dispersion below the Fermi level [Fig.1(F)] it is clear that the central hexagonal FS is formed by a single band (Fermi crossing 1) whereas the dumbbell shaped FSs are formed by the merger of two bands (Fermi crossings 4 and 5) [10].

This band dispersion resembles the partner switching dispersion behavior characteristic of topological insulators. To check this scenario and determine the topological index ν_0, we have carried out spin-resolved photoemission spectroscopy. Fig.1(G) shows a spin-resolved momentum distribution curve taken along the $\bar{\Gamma}$-$\bar{M}$ direction at a binding energy $E_B = -25$ meV [Fig.1(G)]. The data reveal a clear difference between the spin-up and spin-down intensities of bands 1, 2 and 3, and show that bands 1 and 2 have opposite spin whereas bands 2 and 3 have the same spin (detailed analysis discussed later in text). The former observation confirms that bands 1 and 2 form a spin-orbit split pair, and the latter observation suggests that bands 2 and 3 (as opposed to bands 1 and 3) are connected above the Fermi level and form one band. This is further confirmed by directly imaging the bands through raising the chemical potential via doping [see supporting online material (SOM B) [22]]. Irrelevance of bands 2 and 3 to the topology is consistent with the fact that the Fermi surface pocket they form does not enclose any $\vec{k}_T$. Because of a dramatic intrinsic weakening of signal intensity near crossings 4 and 5, and the small energy and momentum splittings of bands 4 and 5 lying at the resolution limit of modern spin-resolved ARPES spectrometers, no conclusive spin information about these two bands can be drawn from the methods employed in obtaining the data sets in Figs 1(G)&(H). However, whether bands 4 and 5 are both singly or doubly degenerate does not change the fact that an odd number of spin-polarized FSs enclose the $\vec{k}_T$, which provides evidence that $Bi_{1-x}Sb_x$ has $\nu_0 = 1$ and that its surface supports a non-trivial Berry's phase.

We investigated the quantum origin of topological order in this class of materials. It has been theoretically speculated that the novel topological order originates from the parities

of the electrons in pure Sb and not Bi [11,23]. It was also noted [20] that the origin of the topological effects can only be tested by measuring the spin-texture of the Sb surface, which has not been measured. Based on quantum oscillation and magneto-optical studies, the bulk band structure of Sb is known to evolve from that of insulating $Bi_{1-x}Sb_x$ through the hole-like band at H rising above E_F and the electron-like band at L sinking below E_F [23]. The relative energy ordering of the L_a and L_s states in Sb again determines whether the surface state pair emerging from $\bar{\Gamma}$ switches partners [Fig.2(A)] or not [Fig.2(B)] between $\bar{\Gamma}$ and $\bar{M}$, and in turn determines whether they support a non-zero Berry's phase.

In a conventional spin-orbit metal such as gold, a free-electron like surface state is split into two parabolic spin-polarized sub-bands that are shifted in $\vec{k}$-space relative to each other [18]. Two concentric spin-polarized Fermi surfaces are created, one having an opposite sense of in-plane spin rotation from the other, that enclose $\bar{\Gamma}$. Such a Fermi surface arrangement, like the schematic shown in figure 2(B), does not support a non-zero Berry's phase because the $\vec{k}_T$ are enclosed an even number of times (2 for most known materials).

However, for Sb, this is not the case. Figure 2(C) shows a spin-integrated ARPES intensity map of Sb(111) from $\bar{\Gamma}$ to $\bar{M}$. By performing a systematic incident photon energy dependence study of such spectra, previously unavailable with He lamp sources [24], it is possible to identify two V-shaped surface states (SS) centered at $\bar{\Gamma}$, a bulk state located near $k_x = -0.25$ Å^{-1} and resonance states centered about $k_x = 0.25$ Å^{-1} and $\bar{M}$ that are hybrid states formed by surface and bulk states [19] (SOM C [22]). An examination of the ARPES intensity map of the Sb(111) surface and resonance states at E_F [Fig.2(E)] reveals that the central surface FS enclosing $\bar{\Gamma}$ is formed by the inner V-shaped SS only. The outer V-shaped SS on the other hand forms part of a tear-drop shaped FS that does *not* enclose $\bar{\Gamma}$, unlike the case in gold. This tear-drop shaped FS is formed partly by the outer V-shaped SS and partly by the hole-like resonance state. The electron-like resonance state FS enclosing $\bar{M}$ does not affect the determination of ν_0 because it must be doubly spin degenerate (SOM D [22]). Such a FS geometry [Fig.2(G)] suggests that the V-shaped SS pair may undergo a partner switching behavior expected in Fig.2(A). This behavior is most clearly seen in a cut taken along the $\bar{\Gamma}$-$\bar{K}$ direction since the top of the bulk valence band is well below E_F [Fig.2(F)] showing only the inner V-shaped SS crossing E_F while the outer V-shaped SS bends back towards the bulk valence band near $k_x = 0.1$ Å^{-1} before reaching E_F. The additional support for this band dispersion behavior comes from tight

binding surface calculations on Sb [Fig.2(D)], which closely match with experimental data below E_F. Our observation of a single surface band forming a FS enclosing $\bar{\Gamma}$ suggests that pure Sb is likely described by $\nu_0 = 1$, and that its surface may support a Berry's phase.

Confirmation of a surface π Berry's phase rests critically on a measurement of the relative spin orientations (up or down) of the SS bands near $\bar{\Gamma}$ so that the partner switching is indeed realized, which cannot be done without spin resolution. Spin resolution was achieved using a Mott polarimeter that measures two orthogonal spin components of a photoemitted electron [27,28]. These two components are along the y' and z' directions of the Mott coordinate frame, which lie predominantly in and out of the sample (111) plane respectively. Each of these two directions represents a normal to a scattering plane defined by the photoelectron incidence direction on a gold foil and two electron detectors mounted on either side (left and right) [Fig.3(A)]. Strong spin-orbit coupling of atomic gold is known to create an asymmetry in the scattering of a photoelectron off the gold foil that depends on its spin component normal to the scattering plane [28]. This leads to an asymmetry between the left intensity $(I^L_{y',z'})$ and right intensity $(I^R_{y',z'})$ given by $A_{y',z'} = (I^L_{y',z'} - I^R_{y',z'})/(I^L_{y',z'} + I^R_{y',z'})$, which is related to the spin polarization $P_{y',z'} = (1/S_{eff}) \times A_{y',z'}$ through the Sherman function $S_{eff} = 0.085$ [27,28]. Spin-resolved momentum distribution curve data sets of the SS bands along the $-\bar{M}$-$\bar{\Gamma}$-$\bar{M}$ cut at $E_B = -30$ meV [Fig.3(B)] are shown for maximal intensity. Figure 3(D) displays both y' and z' polarization components along this cut, showing clear evidence that the bands are spin polarized, with spins pointing largely in the (111) plane. In order to estimate the full 3D spin polarization vectors from a two component measurement (which is not required to prove the partner switching or the Berry's phase), we fit a model polarization curve to our data following the recent demonstration in Ref-[26], which takes the polarization directions associated with each momentum distribution curve peak [Fig.3(C)] as input parameters, with the constraint that each polarization vector has length one (in angular momentum units of $\hbar/2$). Our fitted polarization vectors are displayed in the sample (x, y, z) coordinate frame [Fig.3(F)], from which we derive the spin-resolved momentum distribution curves for the spin components parallel $(I^\uparrow_y)$ and anti-parallel $(I^\downarrow_y)$ to the y direction (SOM B [22]) as shown in figure 3(E). There is a clear difference in $I^\uparrow_y$ and $I^\downarrow_y$ at each of the four momentum distribution curve peaks indicating that the surface state bands are spin polarized [Fig.3(E)], which is possible to conclude even without a full 3D fitting. Each of the pairs $l2/l1$ and $r1/r2$ have opposite spin, consistent with the behavior of a spin split pair, and the spin

polarization of these bands are reversed on either side of $\bar{\Gamma}$ in accordance with the system being time reversal symmetric $[E(\vec{k},\uparrow) = E(-\vec{k},\downarrow)]$ [Fig.3(F)]. The measured spin texture of the Sb(111) surface states (Fig.3), together with the connectivity of the surface bands (Fig.2), uniquely determines its belonging to the $\nu_0 = 1$ class. Therefore the surface of Sb carries a non-zero (π) Berry's phase via the inner V-shaped band and pure Sb can be regarded as the parent metal of the $Bi_{1-x}Sb_x$ topological insulator class, in other words, the topological order originates from the Sb wave functions.

Our spin polarized measurement methods (Fig.1 and 3) uncover a new type of topological quantum number n_M which provides information about the chirality properties. Topological band theory suggests that the bulk electronic states in the mirror ($k_y = 0$) plane can be classified in terms of a number n_M ($=\pm 1$) that describes the handedness (either left or right handed) or chirality of the surface spins which can be directly measured or seen in spin-resolved experiments [20]. We now determine the value of n_M from our data. From figure 1, it is seen that a single (one) surface band, which switches partners at $\bar{M}$, connects the bulk valence and conduction bands, so $|n_M| = 1$ (SOM F [22]). The sign of n_M is related to the direction of the spin polarization $\langle\vec{P}\rangle$ of this band [20], which is constrained by mirror symmetry to point along $\pm\hat{y}$. Since the central electron-like FS enclosing $\bar{\Gamma}$ intersects six mirror invariant points [see Fig.3(B)], the sign of n_M distinguishes two distinct types of handedness for this spin polarized FS. Figures 1(F) and 3 show that for both $Bi_{1-x}Sb_x$ and Sb, the surface band that forms this electron pocket has $\langle\vec{P}\rangle \propto -\hat{y}$ along the k_x direction, suggesting a left-handed rotation sense for the spins around this central FS thus $n_M = -1$. Therefore, both insulating $Bi_{1-x}Sb_x$ and pure Sb possess equivalent chirality properties − a definite spin rotation sense (left-handed chirality, see Fig.3(B)) and a topological Berry's phase.

These spin-resolved experimental measurements reveal an intimate and straightforward connection between the topological quantum numbers (ν_0, n_M) and the physical observables. The ν_0 determines whether the surface electrons support a non-trivial Berry's phase, and if they do, the n_M determines the spin handedness of the Fermi surface that manifests this Berry's phase. The 2D Berry's phase is a critical signature of topological order and is not realizable in isolated 2D electron systems, nor on the surfaces of conventional spin-orbit or exchange coupled magnetic materials. A non-zero Berry's phase is known, theoretically, to protect an electron system against the almost universal weak-localization behavior in

their low temperature transport [11,13] and is expected to form the key element for fault-tolerant computation schemes [13,29, 30]. Its remarkable realization on the $Bi_{1-x}Sb_x$ surface represents an unprecedented example of a 2D π Berry's phase, and opens the possibility for building realistic prototype systems to test quantum computing modules.

In summary, using Mott polarimetry, for the first time we probed the spin degrees of freedom of these quantum spin Hall states and demonstrated that topological quantum numbers are uniquely determined from spin texture imaging measurements. Applying this method to the $Bi_{1-x}Sb_x$ series, we identified the origin of its novel order and unusual chiral properties. These results taken together constitute the first observation of surface electrons collectively carrying a geometrical quantum Berry's phase and definite chirality (topological mirror Chern number $n_M =$-1), which are the key electronic properties for realizing topological computing bits with intrinsic spin Hall-like topological phenomena. Our spin-resolved results not only provides the first clear proof of a topological insulating state in nature but also demonstrate the utility of spin-resolved ARPES technique in measuring the quantum spin Hall phases of matter. Our results as demonstrated here thus open up a new search front for topological quantum materials for novel spin-devices and paves a new way to achieving fault-tolerant quantum computing.

---

[1] N. W. Ashcroft, N. D. Mermin, *Solid State Physics* (Holt, Rinehart and Winston, New York, 1976).

[2] K. v. Klitzing, G. Dorda, M. Pepper, *Phys. Rev. Lett.* **45**, 494 (1980).

[3] R. B. Laughlin, *Phys. Rev. Lett.* **50**, 1395 (1983).

[4] X. -G. Wen, *Int. J. Mod. Phys. B* **4**, 239 (1990).

[5] D. J. Thouless *et al.*, *Phys. Rev. Lett.* **49**, 405 (1982).

[6] J. E. Avron, D. Osadchy, R. Seiler, *Phys. Today* **56** (8), 38 (2003).

[7] M. König *et al.*, *Science* **318**, 766 (2007).

[8] B. A. Bernevig, T. L. Hughes, S. -C. Zhang, *Science* **314**, 1757 (2006).

[9] N. Nagaosa, *Science* **318**, 758 (2007).

[10] D. Hsieh, D. Qian, L. Wray, Y. Xia, Y.S. Hor, R.J. Cava, M.Z. Hasan *Nature* **452**, 970 (2008).

[11] L. Fu, C. L. Kane, *Phys. Rev. B* **76**, 045302 (2007).

[12] X. -L. Qi, T. Hughes, S. -C. Zhang, *Phys. Rev. B* **78**, 195424 (2008).

[13] L. Fu, C. L. Kane, *Phys. Rev. Lett.* **100**, 096407 (2008).

[14] C. L. Kane, E. J. Mele, *Phys. Rev. Lett.* **95**, 146802 (2005).

[15] J. E. Moore, L. Balents, *Phys. Rev. B* **75**, 121306(R) (2007).

[16] J. J. Sakurai, *Modern Quantum Mechanics* (Addison-Wesley, New York, 1994).

[17] M. V. Berry, *Proc. R. Soc. London Ser. A* **392**, 45 (1984).

[18] M. Hoesch *et al.*, *Phys. Rev. B* **69**, 241401(R) (2004).

[19] S. Hufner, *Photoelectron Spectroscopy* (Springer-. verlag, Berlin, 1995).

[20] J. C. Y. Teo, L. Fu, C. L. Kane, *Phys. Rev. B* **78**, 045426 (2008).

[21] T. Hirahara *et al.*, *Phys. Rev. B* **76**, 153305 (2007).

[22] See Materials and methods.

[23] B. Lenoir *et al.*, *Fifteenth International Conference on Thermoelectrics*, 1-13 (1996).

[24] K. Sugawara *et al.*, *Phys. Rev. Lett.* **96**, 046411 (2006).

[25] Y. Liu, E. Allen, *Phys. Rev. B* **52**, 1566 (1995).

[26] F. Meier *et al.*, *Phys. Rev. B* **77**, 165431 (2008).

[27] M. Hoesch *et al.*, *J. Electron Spectrosc. Relat. Phenom.* **124**, 263 (2002).

[28] T. J. Gay, F. B. Dunning, *Rev. Sci. Instrum.* **63**, 1635 (1992).

[29] P. J. Leek *et al.*, *Science* **318**, 1889 (2007).

[30] A. Kitaev, *Ann. Phys. (NY)* **303**, 2 (2003).

FIG. 1. Theoretical spin spectrum of a topological insulator and spin-resolved spectroscopy results. (A) Schematic sketches of the bulk Brillouin zone (BZ) and (111) surface BZ of the $Bi_{1-x}Sb_x$ crystal series. The high symmetry points $(L,H,T,\Gamma,\bar{\Gamma},\bar{M},\bar{K})$ are identified. (B) Schematic of Fermi surface pockets formed by the surface states (SS) of a topological insulator that carries a Berry's phase. (C) Partner switching band structure topology: Schematic of spin-polarized SS dispersion and connectivity between $\bar{\Gamma}$ and $\bar{M}$ required to realize the FS pockets shown in panel-(B). L_a and L_s label bulk states at L that are antisymmetric and symmetric respectively under a parity transformation (see text). (D) Spin-integrated ARPES intensity map of the SS of $Bi_{0.91}Sb_{0.09}$ at E_F. Arrows point in the measured direction of the spin. (E) High resolution ARPES intensity map of the SS at E_F that enclose the $\bar{M}_1$ and $\bar{M}_2$ points. Corresponding band dispersion (second derivative images) are shown below. The left right asymmetry of the band dispersions are due to the slight offset of the alignment from the $\bar{\Gamma}$-$\bar{M}_1$($\bar{M}_2$) direction. (F) Surface band dispersion image along the $\bar{\Gamma}$-$\bar{M}$ direction showing five Fermi level crossings. The intensity of bands 4,5 is scaled up for clarity (the dashed white lines are guides to the eye). The schematic projection of the bulk valence and conduction bands are shown in shaded blue and purple areas. (G) Spin-resolved momentum distribution curves presented at $E_B = -25$ meV showing single spin degeneracy of bands at 1, 2 and 3. Spin up and down correspond to spin pointing along the $+\hat{y}$ and $-\hat{y}$ direction respectively. (H) Schematic of the spin-polarized surface FS observed in our experiments. It is consistent with a $\nu_0 = 1$ topology (compare (B) and (H)).

FIG. 2. Topological character of pure Sb revealed on the (111) surface states. Schematic of the bulk band structure (shaded areas) and surface band structure (red and blue lines) of Sb near E_F for a (A) topologically non-trivial and (B) topological trivial (gold-like) case, together with their corresponding surface Fermi surfaces are shown. (C) Spin-integrated ARPES spectrum of Sb(111) along the $\bar{\Gamma}$-$\bar{M}$ direction. The surface states are denoted by SS, bulk states by BS, and the hole-like resonance states and electron-like resonance states by h RS and e^- RS respectively. (D) Calculated surface state band structure of Sb(111) based on the methods in [20,25]. The continuum bulk energy bands are represented with pink shaded regions, and the lines show the discrete bands of a 100

layer slab. The red and blue single bands, denoted Σ_1 and Σ_2, are the surface states bands with spin polarization $\langle \vec{P} \rangle \propto +\hat{y}$ and $\langle \vec{P} \rangle \propto -\hat{y}$ respectively. (E) ARPES intensity map of Sb(111) at E_F in the k_x-k_y plane. The only one FS encircling $\bar{\Gamma}$ seen in the data is formed by the inner V-shaped SS band seen in panel-(C) and (F). The outer V-shaped band bends back towards the bulk band best seen in data in panel-(F). (F) ARPES spectrum of Sb(111) along the $\bar{\Gamma}$-$\bar{K}$ direction shows that the outer V-shaped SS band merges with the bulk band. (G) Schematic of the surface FS of Sb(111) showing the pockets formed by the surface states (unfilled) and the resonant states (blue and purple). The purely surface state Fermi pocket encloses only one Kramers degenerate point $(\vec{k}_T)$, namely, $\bar{\Gamma}(=\vec{k}_T)$, therefore consistent with the $\nu_0 = 1$ topological classification of Sb which is different from Au (compare (B) and (G)). As discussed in the text, the hRS and e^-RS count trivially.

FIG. 3. **Spin-texture of topological surface states and chirality.** (A) Experimental geometry of the spin-resolved ARPES study. At normal emission ($\theta = 0°$), the sensitive y'-axis of the Mott detector is rotated by $45°$ from the sample $\bar{\Gamma}$ to $-\bar{M}$ ($\parallel -\hat{x}$) direction, and the sensitive z'-axis of the Mott detector is parallel to the sample normal ($\parallel \hat{z}$). (B) Spin-integrated ARPES spectrum of Sb(111) along the $-\bar{M}$-$\bar{\Gamma}$-$\bar{M}$ direction. The momentum splitting between the band minima is indicated by the black bar and is approximately 0.03 Å^{-1}. A schematic of the spin chirality of the central FS based on the spin-resolved ARPES results is shown on the right. (C) Momentum distribution curve of the spin averaged spectrum at $E_B = -30$ meV (shown in (B) by white line), together with the Lorentzian peaks of the fit. (D) Measured spin polarization curves (symbols) for the detector y' and z' components together with the fitted lines using the two-step fitting routine [26]. (E) Spin-resolved spectra for the sample y component based on the fitted spin polarization curves shown in (D). Up (down) triangles represent a spin direction along the $+(-)\hat{y}$ direction. (F) The in-plane and out-of-plane spin polarization components in the sample coordinate frame obtained from the spin polarization fit. Overall spin-resolved data and the fact that the surface band that forms the central electron pocket has $\langle \vec{P} \rangle \propto -\hat{y}$ along the $+k_x$ direction, as in (E), suggest a left-handed chirality (schematic in (B) and see text for details).
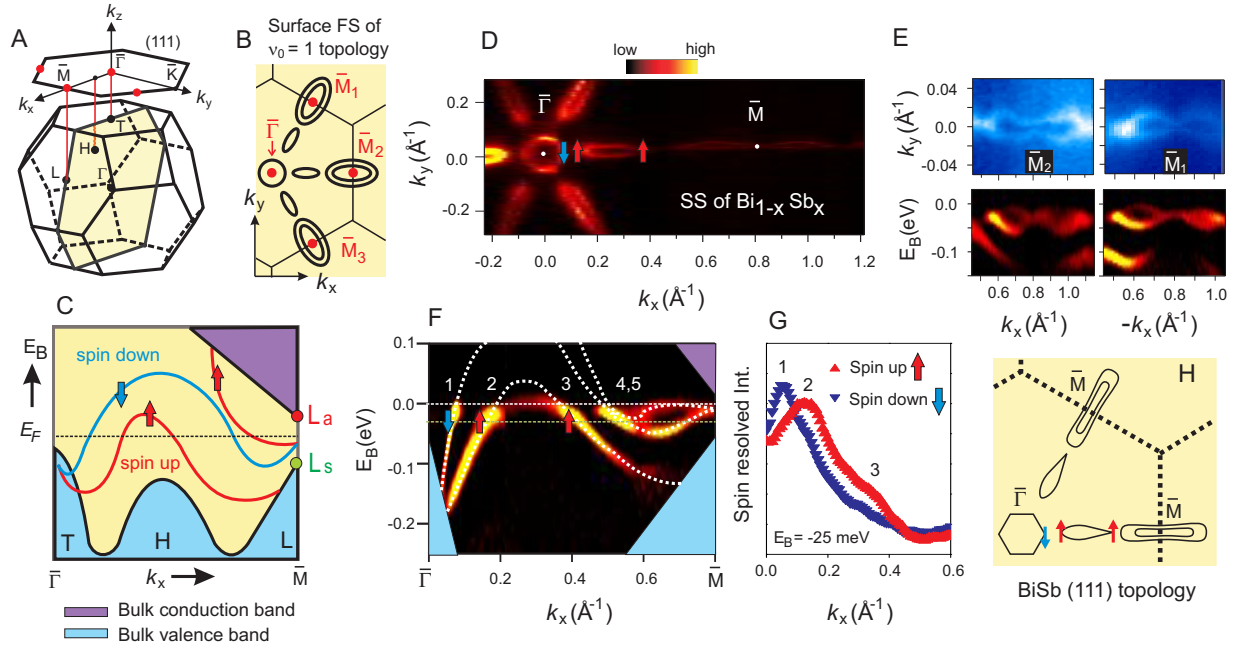
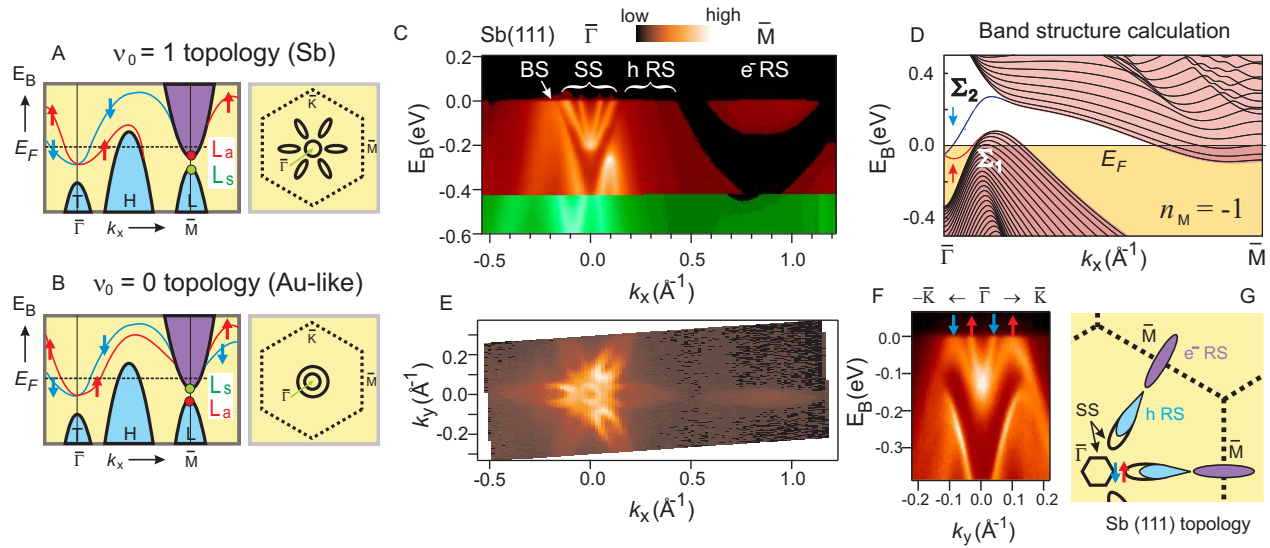FIG. 1: D. Hsieh *et al*. SCIENCE 323, 919 (2009) [Princeton University]

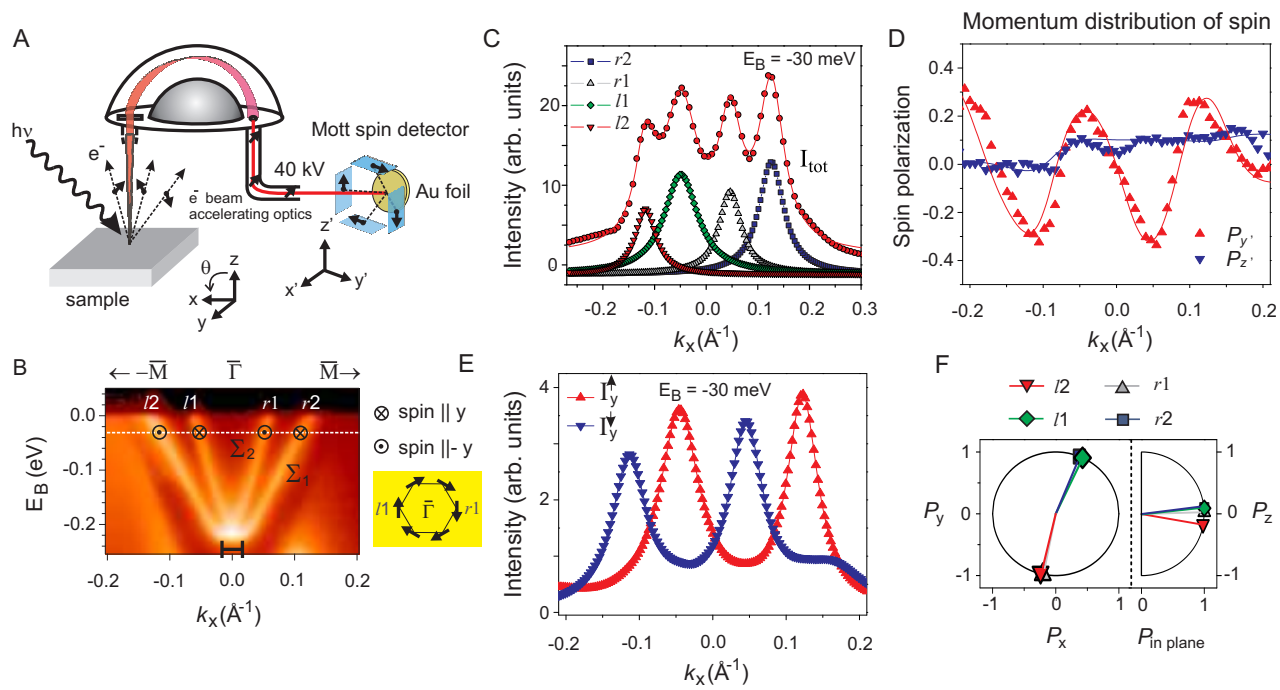FIG. 2: D. Hsieh *et al.* SCIENCE 323, 919 (2009) [Princeton University]

FIG. 3: D. Hsieh *et al.* SCIENCE 323, 919 (2009) [Princeton University]